

Software for Automatic Detection and Monitoring of Fluorescent Lesions in Mice

S. Foucher, M. Lalonde, L. Gagnon
Computer Research Institute of Montreal, Montreal (QC), Canada
{sfoucher, mlalonde, lgagnon}@crim.ca

A.-M. Steff
World Anti-Doping Agency, Montreal (QC), Canada
ann-muriel.steff@wada-ama.org

Abstract

Detection and monitoring of fluorescent lesions in mice is usually performed manually with the help of an image manipulation commercial software. The task is often daunting due to the huge amount of images and the degradation of the fluorescent signal over time. We developed a software aiming at automatically detecting lesions based on a color analysis and segmentation of the images. The software offers tools to assess the fluorescence decay rate over time using robust regression techniques.

1. Introduction

The main goal of the proposed software is to automatically detect and estimate surfaces of fluorescent endometrial fragments in mice based on a color analysis and segmentation of images. Detection is particularly difficult for a human operator at the end of the fluorescence lifetime when the signal to noise ratio is weak and the lesion surfaces small. A second purpose was to offer tools to assess the fluorescence decay rate over time using robust regression techniques.

In nature, green fluorescent protein (GFP) is produced by *Aequorea victoria*, the Pacific Northwest jellyfish. The protein has become of great interest to cell and molecular biologists because it can reveal gene expression in living cells. This is done by linking the gene for GFP to the gene whose expression you are interested in. When that gene is turned on in a cell, not only is its protein synthesized, but GFP is synthesized as well. Illuminating the cells with near-ultraviolet light causes the cell to fluoresce a bright green. In this way, the experimenter can see when and where the gene is expressed in the living organism. In the case of experimental endometriosis, human endometrial tissue is genetically modified to express GFP and transplanted into immunodeficient mice. This model represents a valuable preclinical tool for testing the efficiency of new drugs targeting endometriosis [1-2].

The development of endometriotic lesions can be monitored through direct visualization of fluorescent tissue in the living animal. Several pictures are taken with the help of a digital camera over a period of 20 days. The developed software aims at identify in each image four types of objects (tissue, fluorescent endometrial fragments,

background and an optional fluorescent target). Following this segmentation step, the number of pixels belonging to the lesion is estimated and included into a robust regression model.

2. Experimental settings

The mice are observed during a period of 20-25 days. At each time point, several images are taken (usually 3 to 4) in order to reduce the noise due mainly to unexpected motion and variation in the viewpoint. The targets are illuminated by a special source equipped with a 470nm filter and 2048x2048 color images are recorded with a digital camera mounted with a 515nm viewing filter. Further details can be found in [1]. We consider three classes: normal tissue, endometrial fragments (fluorescent lesions) and background (a fourth target is also present which is an artificial target exhibiting a fluorescent-like signature).

3. Fluorescent lesion extraction method

3.1. Color analysis

A preliminary study was performed to analyze the color signature of the different targets in the Red-Green-Blue (RGB) space in order to assess if the fluorescent tissue exhibits a discriminant color signature. We measured the color separability between fluorescent lesion and normal tissue samples with the help of the Bhattacharyya distance [3]:

$$B = \frac{1}{8} (\bar{\mathbf{I}}_T - \bar{\mathbf{I}}_L)^T \left\{ \frac{1}{2} (\boldsymbol{\Sigma}_T + \boldsymbol{\Sigma}_L) \right\}^{-1} (\bar{\mathbf{I}}_T - \bar{\mathbf{I}}_L) + \frac{1}{2} \ln \left(\frac{(\boldsymbol{\Sigma}_T + \boldsymbol{\Sigma}_L) / 2}{|\boldsymbol{\Sigma}_T| |\boldsymbol{\Sigma}_L|} \right) \quad (1)$$

where $\bar{\mathbf{I}}_T$ and $\boldsymbol{\Sigma}_T$ (resp. $\bar{\mathbf{I}}_L$ and $\boldsymbol{\Sigma}_L$) are the mean value and the covariance matrix in the RGB color space for the normal tissue (resp. for the fluorescent lesion). These distances are estimated at different time intervals and are shown in Table 1. Most of the values are above 2.0 which is a lower bound value for considering the target signatures as distinct [3]. The most discriminant color is the green color and the best combinations are RGB and RG. Moreover, the color signature is still discriminant at the end of the fluorescence lifetime.

Table 1. Bhattacharyya distances evaluated with different color combinations and five mice over a twenty day period.

Day	R	G	B	RG	RB	GB	RGB
1	1.78	14.71	1.46	26.39	3.15	17.70	34.00
4	0.75	12.21	1.34	20.26	2.33	19.45	29.49
6	0.95	7.54	0.80	13.29	1.02	9.31	20.30
8	0.48	9.41	1.86	21.32	5.11	34.84	35.05
12	3.95	4.19	0.65	7.49	4.60	8.71	10.25
15	0.13	3.91	0.32	3.86	0.33	4.00	3.91
18	0.21	6.44	0.81	6.61	0.75	7.69	7.69
20	0.79	5.49	0.48	7.03	0.99	6.24	7.51

SEQARABE

Figures 1 and 2 show the corresponding histograms for the samples at day 1 and 20 respectively. We observe that the fluorescence color signature is mainly characterized by a strong difference between the green and the red channels. There are no significant differences between the green and red histograms for normal tissue.

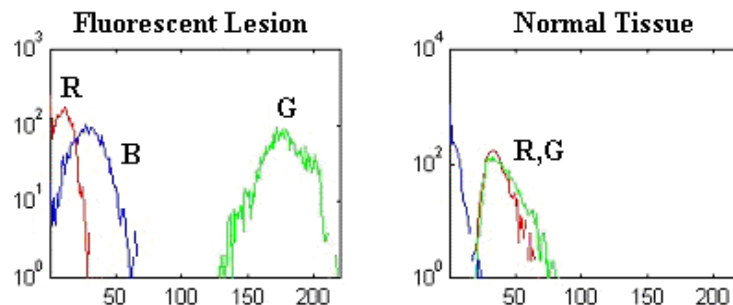


Figure 1. Intensity value distribution in the different color channels for the fluorescent lesion and the normal tissue at day one.

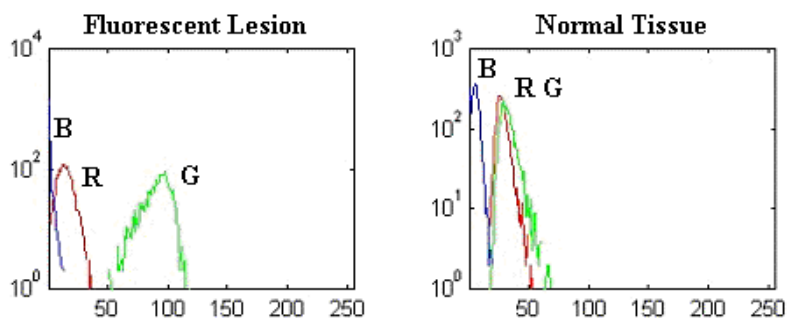


Figure 2. Same as Figure 1 but for day 20.

As a conclusion of this preliminary analysis, we can assume that a two or three color signature is enough to separate fluorescent lesion from normal tissue areas over the course of the fluorescence signal lifetime. As a result, we estimate a color signature for the lesion ($\bar{\mathbf{I}}_L$ and Σ_L) from several images at day one when the fluorescence is the strongest. Additionally, the difference between the green and red channels is a good indicator of fluorescence. This will be used to provide initial segments to the segmentation process described below and to enhance the image for direct inspection on the user interface (see Figure 3.c).

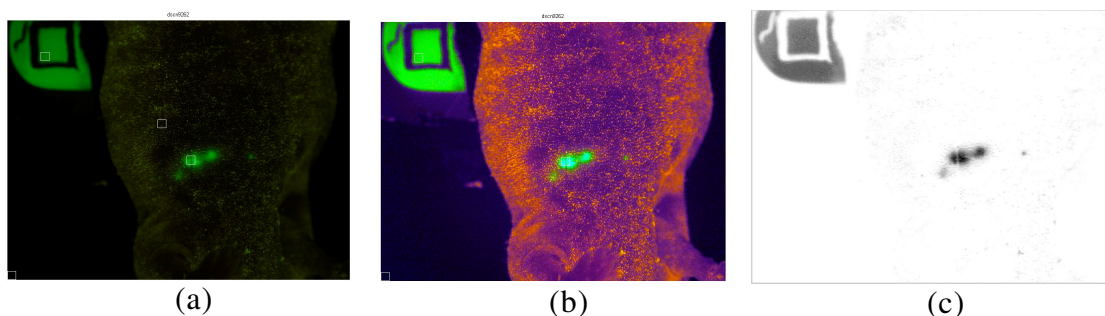


Figure 3. a) Original image; b) Image after linear stretch of the histogram; c) Difference image between the green and red channels.

3.2. Segmentation and region growing

The segmentation process starts with lesion seeds derived from a thresholding of the red-green difference image. We then obtain a preliminary image classification as shown in Figure 4.a. This classification is conservative and leave mixed pixels on lesion borders unclassified (black pixels in Figure 4.a). The next step is to expand these lesion seeds based on the multi-spectral signature for the fluorescence and the tissue. We apply a region growing to expand lesion seeds based on their posterior color likelihood [4] where an unlabelled pixel I is classified as a lesion if the following Bayesian ratio is verified:

$$\frac{\pi_L p(I | \Sigma_L, \bar{I}_L)}{\pi_T p(I | \Sigma_T, \bar{I}_T)} > 1 \quad (2)$$

where π_L and π_T are the a priori probabilities for the lesions and the tissue estimated from the preliminary classification (Figure 4.a). The color signature for the tissue is also derived from the preliminary classification. As a result of this process, we obtain a refined binary classification map for the lesions (Figure 4.b).

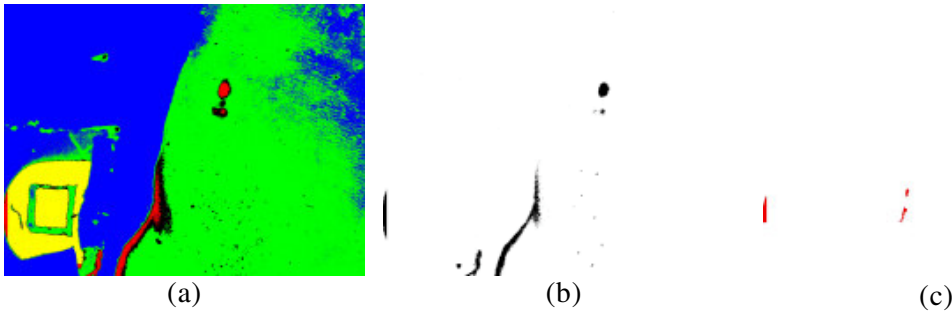


Figure 4. a) Preliminary coarse classification (blue=background, red=lesions, green=tissue, black=unlabelled); b) Result of the region growing around the lesion seeds; c) Result of the filtering process.

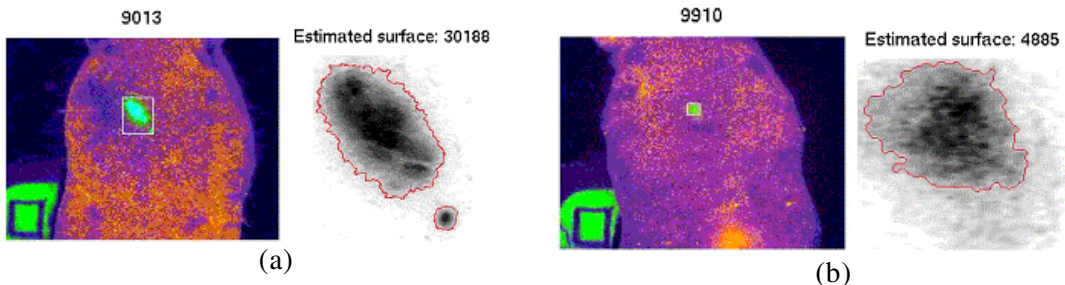


Figure 5. Two results of detection on day 1 (a) and day 20 (b). The detected lesion boundaries are displayed over the difference image between the red and green bands.

From this classification map, we extract individual segments (spatially separated regions). Small segments are then discarded. False alarms frequently occur due, for instance, to the presence of urine which exhibits also a fluorescent signature (as shown at the bottom of Figure 4.b). Therefore, a set of rules is applied to filter out false alarms

based on the fact that lesion segments form a relatively tight group and occur at the center of the mouse body. An example of final segmentation result is shown in Figure 4.c. Regions which do not verify these rules are not suppressed but rather labeled as lesion candidates and displayed in red in the user interface. The lesion contour candidates are then extracted and smoothed as shown in Figure 5.

4. Software Design

The software was designed to enable the user to eventually make corrections in the result by excluding or including lesion segment candidates. The fluorescent spectral signatures can be easily modified in the interface. An important feature, is the regression analysis tool, which displays all the individual estimated surfaces in a log-linear regression model using robust estimation techniques [5]. Each point in this graph is linked to the corresponding image displayed in the main interface (see Figure 6). Furthermore, circle colors within the regression panel are function of the weight attributed by the robust regression algorithm (red= inliers, blue= outliers).

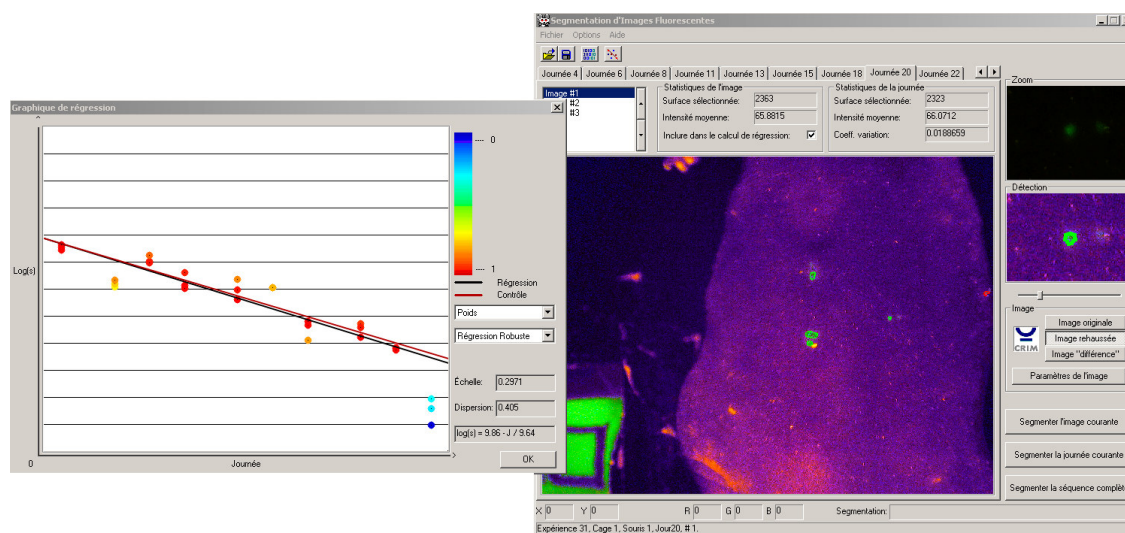


Figure 6. Software interface composed of the regression panel (left) and the main window (right) displaying an individual segmentation result.

5. Evaluation

The proposed software aimed at reducing noise in the estimation of the lesion surface. A way to evaluate the noise level is to calculate the normalized standard deviation of the estimated surfaces (ratio of the standard deviation to the mean) from the set of images of a given mouse acquired at the same time point. We compare results obtain by the proposed method with a manual approach consisting of drawing the lesion boundaries on the green channel of each image using a common photo editing software (see Figure 7). The surface error is decreased by almost a two-order magnitude factor.

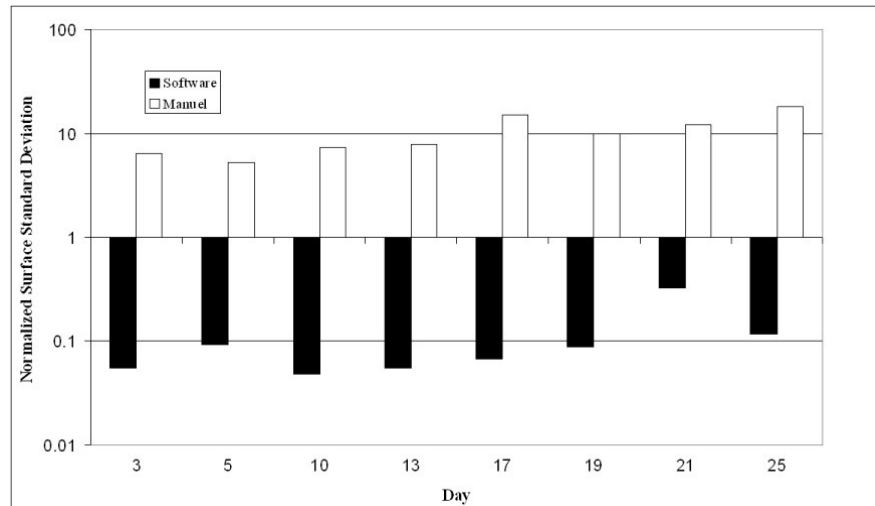


Figure 7. Average normalized standard deviation of the surfaces measured on 4 sequences using the manual method and by the developed software.

6. Discussion and Conclusion

Comparison with manual results shows that detection accuracy was greatly improved especially at the end of the sequence when the fluorescent signal decreases significantly and becomes difficult to visualize for a human operator. The processing of a whole sequence (about 30-50 images) takes about one minute which is a very significant gain compared to manual processing. Finally, the simultaneous visualization of the regression results and the detected segments enables the user to make corrections based on the overall statistical behavior of the sequence and to identify outliers more easily.

The developed software aims at automatically detecting fluorescent endometrial fragments in mice and monitoring the fluorescent signature decay over time. The main purpose is to improve detection results, facilitate the work and increase the productivity of lab technicians.

References

- [1] Fortin, M., Lépine, M., Merlen, Y., Thilbeault, I., Rancourt, C., Gosselin, D., Hugo, P. and Steff, A.-M., "Quantitative Assessment of Human Endometriotic Tissue Maintenance and Regression in a Noninvasive Mouse Model of Endometriosis", *Mol. Ther.* 2004, 9(4):540-547.
- [2] Steff, A.-M., Fortin, M., Massie, B., Hugo, P., "Establishment of an improved mouse model of endometriosis allowing the non-invasive assessment of implantation, progression and regression of human endometriotic lesions". *Fertil Steril.* 2003; 80(Suppl 2):832-838.
- [3] Richards, J. and Jia, X., "Remote Sensing Digital Image Analysis : An introduction", Third Edition, Springer.
- [4] Duda, R.O., Hart, P.E. and Stork, D.G., "Pattern Classification", John Wiley & Sons, 2nd edition, 2001.
- [5] Holland, P.W., and Welsch, R.E., "Robust Regression Using Iteratively Reweighted Least-Squares", *Communications in Statistics: Theory and Methods*, A6, pp. 813-827, 1977.